Theoretical Study of the Electronic Structure of [Tetrathiafulvalene]$_2^{2+}$ Dimers and Their Long, Intradimer Multicenter Bonding in Solution and the Solid State

Iñigo Garcia-Yoldi,[†] Joel S. Miller,*[,‡] and Juan J. Novoa*[,†]

Departament de Química Física and IQTCUB, Facultat de Química, Universitat de Barcelona, Av. Diagonal 647, 08028 Barcelona, Spain, and Department of Chemistry, University of Utah, Salt Lake City, Utah 84112-0850

Received: August 06, 2008; Revised Manuscript Received: October 24, 2008

The long, multicenter bonding in tetrathiafulvalenium cation radical dimers, $[TTF]_2^{2+}$, observed in both the solid state and in solution, were computationally investigated via B3LYP, CASSCF(2,2), and MCQDPT/CASSCF(2,2) calculations. The stability of $[TTF]_2^{2+}$ dimers originates from $[TTF]^{\bullet+}\cdots$anion$^-$ or $[TTF]^{\bullet+}\cdots$solvent electrostatic interactions, whose sum exceeds the $[TTF]^{\bullet+}\cdots[TTF]^{\bullet+}$ repulsion, in solution, or the sum of the $[TTF]^{\bullet+}\cdots[TTF]^{\bullet+}$ and anion$^-\cdots$anion$^-$ repulsions in solid state. MCQDPT/CASSCF(2,2) calculations indicate that the electronic ground state of the $[TTF]_2^{2+}$ dimers is a closed-shell single state with non-negligible contribution of the open-shell singlet, as is experimentally observed. This ground state is not well reproduced in B3LYP or CASSCF(2,2) calculations.

Introduction

The presence of long C−C bonds between anion radicals that exhibit all of the electronic properties of a conventional covalent bond, except for its intrinsic energetic stability, was first reported in salts of reduced tetracyanoethylene (TCNE), where $\pi-[TCNE]_2^{2-}$ dimers are found.[1−10] The dimer stability originates from the cation$^+\cdots[TCNE]^{\bullet-}$ attractive interactions, which overcome the anion$\cdots$anion plus cation$\cdots$cation repulsive interactions (there is also a smaller extra stabilization coming from the dispersion energetic component[11]), and the intradimer C−C distance is ∼2.9 Å. At this distance the $[TCNE]^{\bullet-}$ b_{2g} singly occupied molecular orbitals (SOMOs) overlap to form b_{2u} $[TCNE]_2^{2-}$ bonding and b_{1g} antibonding orbitals that are, respectively, doubly occupied and empty in the singlet ground state. Hence, $[TCNE]_2^{2-}$ has the same orbital diagram as that for conventional covalent bonds.

$[TCNE]_2^{2-}$ is prototypical of an increasing number of organic compounds that are best described by long, multicenter bonding. In addition to other anions (e.g., cyanil[12] and 7,7,8,8-tetracyano-*p*-quinodimethane (TCNQ)[4,13−18]) examples include cations, e.g., $[TTF]_2^{2+}$ (tetrathiafulvalene)$_2^{2+}$, as well as neutral radicals. Several examples of salts possessing nominally cofacial $\pi-[TTF]_2^{2+}$ dimers have been reported.[19−32] These dimers have the shortest interfragment C−C distance, ∼3.5 Å, which is less than the sum of the van der Waals radii of sulfur.[33]

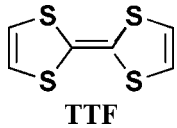

TTF

The formation of $[TTF]_2^{2+}$ dimers was also reported in water[34] and ethanol[35] solutions at very low temperature. Spectroscopic (UV−vis and electron paramagnetic resonance (EPR)) studies in various solvents have established the thermodynamic parameters for the cation radical dimerization in ethanol, acetone, dimethylformamide (DMF), acetonitrile (MeCN), tetrahydrofuran (THF), and dichloromethane.[36] The weakest association was found in dichloromethane, where $\Delta H_{dim} = -3.8$ kcal/mol and $\Delta S_{dim} = -18$ eu. The $2[TTF]^{\bullet+} \rightleftarrows [TTF]_2^{2+}$ dimerization process was found to be reversible, but solvent- and temperature-dependent, and less than −70 °C is required to observe the dimer in dichloromethane. At −90 °C the absorption spectrum is similar to the reported spectrum of solid $[TTF]_2^{2+}$,[19−21] being essentially invariant when the solvent or counterions were changed. This suggests that the structure of the $[TTF]_2^{2+}$ dimers is similar in solution and the crystal, and also largely unaffected by the environment, as occurs for $[TCNE]_2^{2-}$.

To gain insight into the nature of the intradimer $[TTF]_2^{2+}$ bonding with emphasis on the long C−C separations, the electronic structure of $[TTF]_2^{2+}$, as reported for the representative $[TTF]_2[ClO_4]_2$[20,21] salt has been studied by combining B3LYP density functional, CASSCF(2,2), and MCQDPT/CASSCF(2,2) calculations.

Methodological Details

The characterization of the electronic structure and properties of $[TTF]_2^{2+}$ dimers was executed in three consecutive steps. First, the interaction energy curve of an isolated $[TTF]_2^{2+}$ dimer as a function of the shortest interfragment C−C distance was evaluated at the B3LYP density functional,[37] CASSCF(2,2), and MCQDPT/CASSCF(2,2) computational levels. Second, the energetic interactions in a representative crystal possessing $[TTF]_2^{2+}$ dimers were evaluated in order to identify the reasons behind the existence of the dimers in solids. The energetic evaluation was done on the $[TTF]_2[anion]_2$ aggregate, the smallest aggregate where all the interactions found in the $[TTF]_2[ClO_4]_2$ crystal are present. Finally, the presence of $[TTF]_2^{2+}$ dimers in solution was investigated by evaluating the intermolecular interactions in $[TTF]_2[CH_2Cl_2]_n$ aggregates.[20,21] The electronic structure of the $[TTF]_2^{2+}$ dimers in these calculations will be rationalized in terms of the qualitative orbital

* Corresponding authors. E-mail: juan.novoa@ub.edu (J.J.N.), jsmiller@chem.utah.edu (J.S.M.).
[†] Universitat de Barcelona.
[‡] University of Utah.

10.1021/jp807022h CCC: $40.75
Published on Web 12/22/2008

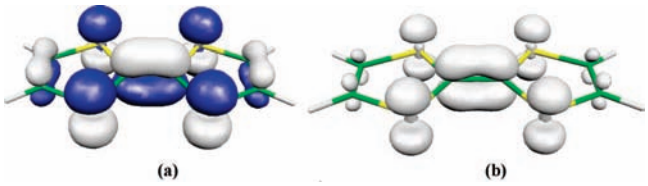

Figure 1. (a) Shape of the SOMO of $[TTF]^{\bullet+}$ (S is yellow, C is green, and H is white) computed at the UB3LYP/6-31+G(d) level; (b): shape of the spin density (the isosurface of ±0.05 au is plotted; notice the absence of regions of negative electron density).

diagrams that result from the overlap of the SOMO of two $[TTF]^{\bullet+}$ monomers (whose shape was obtained from UB3LYP/6-31+G(d) computations).

The CASSCF(2,2) and MCQDPT/CASSCF(2,2) methods were used because previous B3LYP computations on $[TCNE]_2^{2-}$ dimers failed to reproduce their diamagnetic ground state, a property that is well reproduced by MCQDPT/CASSCF(2,2) calculations. The MCQDPT/CASSCF(2,2) method performs multiconfigurational perturbation calculation on a multiconfigurational CASSCF(2,2) wave function using the MCQDPT method.[38] The MCQDPT/CASSCF(2,2) method provides an accurate evaluation of the dispersion component of the interaction energy and gives results similar to those obtained using the more popular CASPT2 method.[39] In these CASSCF(2,2), and MCQDPT/CASSCF(2,2) calculations the (2,2) active space included the two SOMO orbitals of the fragments at dissociation. In this form, the closed-shell singlet, CSS, and open-shell singlet, OSS, states that can originate from the interaction of the two doublet radical cations can be properly described.

All B3LYP calculations were done using the 6-31+G(d) basis set[40] and the Gaussian-03 suite of programs,[41] while the CASSCF(2,2) and MCQDPT/CASSCF(2,2) calculations were done using the GAMESS-07 suite of programs.[42] In all cases the interaction energies were corrected by the basis set superposition error (BSSE) using the counterpoise method.[43−46]

Results and Discussion

In order to study the electron structure of $[TTF]_2^{2+}$ dimers, the electronic structure of the $[TTF]^{\bullet+}$ monomer was computed at the UB3LYP/6-31+G(d) level and is illustrated in Figure 1. $[TTF]^{\bullet+}$ has a doublet ground state with its SOMO mostly located at the central CC bond, but also with some delocalized on the S and terminal C(sp^2) atoms, Figure 1. Using this SOMO one can rationalize the properties of the $[TTF]^{\bullet+}\cdots[TTF]^{\bullet+}$ interaction in isolated dimers, in crystals of the perchlorate salt, and in dichloromethane solutions.

1. Nature of the $[TTF]^{\bullet+}\cdots[TTF]^{\bullet+}$ Interactions in Isolated $[TTF]_2^{2+}$ Dimers. The potential energy curves for an isolated $[TTF]_2^{2+}$ computed at the RB3LYP/6-31+G(d) and UB3LYP/6-31+G(d) levels are shown in Figure 2. The curves were obtained by optimizing the geometry of the dimer at each distance d (the shortest central C−C distance). Both curves are energetically unstable with respect to the dissociation of the dimer into its fragments; i.e., $[TTF]_2^{2+} \rightleftarrows 2\ [TTF]^{\bullet+}$. A very small metastable minimum is found in the RB3LYP curve, although it disappears when going into the UB3LYP curve. The shape of curve for $[TTF]_2^{2+}$ is similar to that reported for $[TCNE]_2^{2-}$ but is ∼5 kcal/mol more repulsive, probably due to steric effects induced in the five-membered ring by the fragment approach. The comparison of the RB3LYP and UB3LYP curves with those obtained at the CASSCF(2,2) and MCQDPT/CASSCF(2,2) levels is presented in Figure 3. The curve obtained with the better, latter method is more stable than the others and

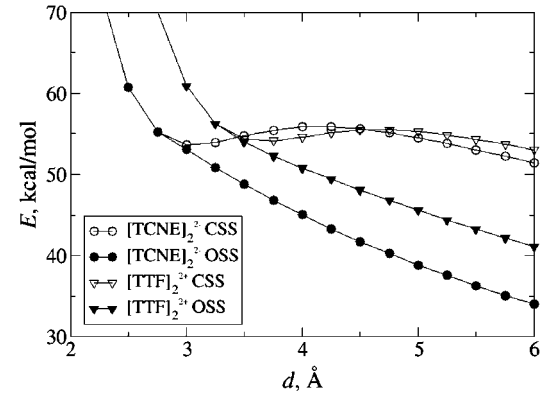

Figure 2. Variation of the interaction energy, E, of two $[TTF]^+$ fragments placed in a D_{2h} geometrical arrangement as a function of interfragment C−C distance (d). The CSS and OSS curves are those for the closed-shell and open-shell singlet states, computed at the RB3LYP and UB3LYP levels, respectively. The equivalent curves computed for the interactions of two $[TCNE]^{\bullet-}$ fragments are also given (refs 1 and 11) for comparison.

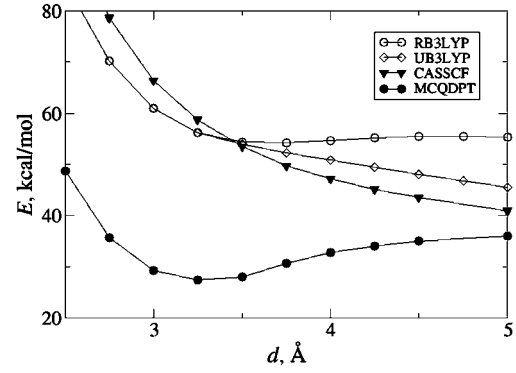

Figure 3. Variation of the interaction energy, E, of two $[TTF]^+$ fragments placed in a D_{2h} geometrical arrangement with the interfragment C−C distance (d) as a function of the computational method. The curves plotted are those obtained using the RB3LYP, UB3LYP, CASSCF(2,2), and MCQDPT/CASSCF(2,2) computational levels.

also has a metastable minimum at ∼3.2 Å that is not found in CASSCF(2,2) calculations. This indicates that the dispersion component of the interaction energy is qualitatively relevant. Thus, independent of method, the formation of isolated $[TTF]_2^{2+}$ dimers requires energy, and it is not a spontaneous process (note, however, that the UB3LYP calculations do not predict a minimum, whereas the RB3LYP and MCQDPT calculations both predict a metastable minimum). Hence, it is only stable when the $[TTF]_2^{2+}$ dimers are in an environment where they can get enough energy to compensate for the intrinsic energetic repulsive nature of their interaction. Thus, the bonding component of the interaction, which originates form the overlap of the two SOMO orbitals of the fragments, is less energetic than the Coulombic $cation^+\cdots cation^+$ component originating from their net positive charges.

2. Nature of the $[TTF]^{\bullet+}\cdots[TTF]^{\bullet+}$ Interactions in Crystals. The existence of pairs of charged radicals in the solid is attributed to the existence of energetically stable aggregates that contain these dimers and whose stability originates in the $cation^+\cdots anion^+$ attractive interactions, which exceeds the sum of the $cation^+\cdots cation^+$ and $anion^-\cdots anion^-$ repulsive interactions. This energetic balance was demonstrated for small $(cation)_2[TCNE]_2$ aggregates[1,11] (Figure 4). These ideas were extended to $[TTF]_2^{2+}$ dimers.

Suitable $[TTF]_2(anion)_2$ aggregates possessing $[TTF]_2^{2+}$ dimers were identified via searching the Cambridge Structural Database

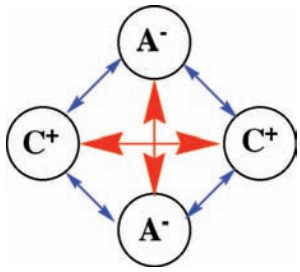

Figure 4. Schematic representation of the most important, first-neighbor pair interactions in $[TTF]_2(anion)_2$ aggregates. Cations are indicated as C^+ and anion as A^-.

(CSD).[47] There are many cases of short distance TTF···TTF pairs, but only a few based on two $[TTF]^{\bullet+}$ monomers, Table 1. Their shortest interfragment C···C distance (d), ∠C···C=C angle (a), and ∠C−C···C−C dihedral angle (θ) are also listed in Table 1. The shortest interfragment C···C distance varies between 3.345 and 3.589 Å, whereas the ∠C···C=C angle varies between 74.4° and 89.5°, and the ∠C−C···C−C dihedral angles ranges between 0.0° and 8.0°. Thus, the geometry of these $[TTF]_2^{2+}$ dimers does not significantly deviate from D_{2h}. Note also that there is a lack of coplanarity between the two five-membered rings of $[TTF]^{\bullet+}$ for some salts.

$[TTF]_2[ClO_4]_2$ was selected for computational study due to the nearly D_{2h} symmetry of its $[TTF]_2^{2+}$ dimers and the small size of its anion.[21] Its crystal packing has stacks of $[TTF]_2^{2+}$ dimers where each pair is surrounded by six perchlorate anions, Figure 5. Within each stack the $[TTF]_2^{2+}$ tilts relative to the c axis. The six ClO_4^- anions are in the equatorial plane of these $[TTF]_2^{2+}$ dimers. The two rings of the $[TTF]^+$ are nearly, but not rigorously, coplanar (∠S−C=C−S is 1.06°). The most energetically stable $[TTF]_2[ClO_4]_2$ aggregate (Figure 6a) was identified by looking at what pair of ClO_4^- anions gave the most stable total energy for the aggregate. The interaction energy of this aggregate, computed at the B3LYP/6-31+G(d) level, is −147.3 kcal/mol for the CSS state, −147.2 kcal/mol for the OSS, and −134.4 kcal/mol for the triplet state. Therefore, at the B3LYP/6-31+G(d) level the ground state of the $[TTF]_2(ClO_4)_2$ aggregate is the closed-shell singlet, although the open-shell singlet state is only 0.1 kcal/mol higher in energy. Note that for the $[TCNE]^{\bullet-}$ [1,5] or $[cyanil]^{\bullet-}$ [12] $(cation)_2(anion)_2$ aggregates the B3LYP functional predicted the open-shell singlet as the ground state.

The origin of the stability of the $[TTF]_2(ClO_4)_2$ aggregate in B3LYP calculations can be traced to the $cation^+\cdots anion^-$ interactions, after comparing the sum of the cation···cation (63.5 kcal/mol) and anion···anion (29.6 kcal/mol) repulsions, with the sum of the cation···anion attractions (−255.8 kcal/mol, which results from adding the following four components: −64.3, −63.3, −60.0, and −68.2). The CSS state of the $[TTF]_2(ClO_4)_2$ aggregate was also found to be −19.7 kcal/mol more stable than its fragmentation into two $[TTF]^{\bullet+}$ and two $(ClO_4)^-$ ions at the crystal geometry (the OSS and triplet states are also more stable than the fragments by −19.6 and −6.8 kcal/mol, respectively).

As a further test of the stability of the $[TTF]_2(ClO_4)_2$ aggregate, its optimum geometry was computed at the RB3LYP/6-31+G(d) level. The RB3LYP optimum geometry has a nearly C_{2h} symmetry, Figure 6b. It is very close to the crystal geometry,

TABLE 1: Shortest Interfragment C···C Distance (d), ∠C=C···C Angle, (a), and ∠C=C···C=C Dihedral Angle (θ) of Structurally Characterized Compounds Possessing $[TTF]_2^{2+}$ Dimers[a]

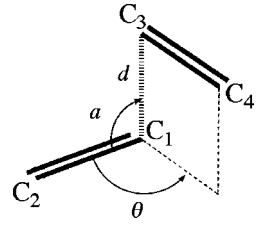

anion, $[TTF]_2(anion)_2$		d, angstroms	a, deg	θ, deg	ref
4-(sulfonatomethylaminocarbonyl)-2,2,6,6-tetramethylpiperidin-1-oxyl dihydrate	CEBWUC	3.421	86.1	0.0	22
4-(2-sulfonatoethylaminocarbonyl)-2,2,6,6-tetramethylpiperidin-1-oxyl monohydrate	CEBXAJ	3.431	85.6	0.0	22
4-(*N*-methyl-2-sulfonatoethylaminocarbonyl)-2,2,6,6-tetramethylpiperidin-1-oxyl hemihydrate	CEBXEN	3.510	84.7	0.0	22
dimethyltrichlorostannate(IV)	DAHYIU	3.388	78.9	0.0	23
ferrocene-1-carbamoyl-*N*-methylsulfonate hydrate	DEBRUV	3.350	83.2	0.0	24
ferrocene-1,1′-dicarbamoyl-*N*,*N*′-bis(methylsulfonate)	DEBSAF	3.471	80.7	4.6	24
tris(bis(pyrazine-2,3-diselenolato))aurate(III)	ECOQIW	3.545	84.4	6.4	25
tris(5,6-dihydro-1,4-dithiine-2,3-dithiolato)vanadate[b]	HAYZUC	3.589	81.5	0.0	26
tris(5,6-dihydro-1,4-dithiine-2,3-dithiolato)vanadate[c]	HAYZUC01	3.521	80.6	0.0	26
2-dicyanomethylene-1,1,3,4,5,5-hexacyanopentenediide	IDAXOA	3.480	74.3	0.0	27
trans-2,2,6,6-tetramethyl-4-((2-sulfonatobenzoyl)oxy)-piperidine-1-oxide	LAYTOV	3.437	87.3	0.0	28
$CF_3SO_3^-$	QIKWEM	3.441	81.8	2.2	29
$[Ta_6Cl_{18}]^{2-}$	SATDEW	3.521	84.3	0.0	30
I_3^-	TTFIOD	3.431	89.5	0.0	31
bis(μ-oxalato)tetrakis(oxalato)diaquadichromium(III)manganese(II)	TUHDOP	3.345	79.8	8.0	32
ClO_4^-	ZZZBWA10	3.439	87.0	3.5	20, 21
maximum		3.589	89.5	8.0	
minimum		3.345	74.4	0.0	
mean		3.458	83.1	1.6	
standard deviation		0.068	3.8	2.7	

[a] The refcode of each crystal[47] is also given. [b] α polymorph. [c] β polymorph.

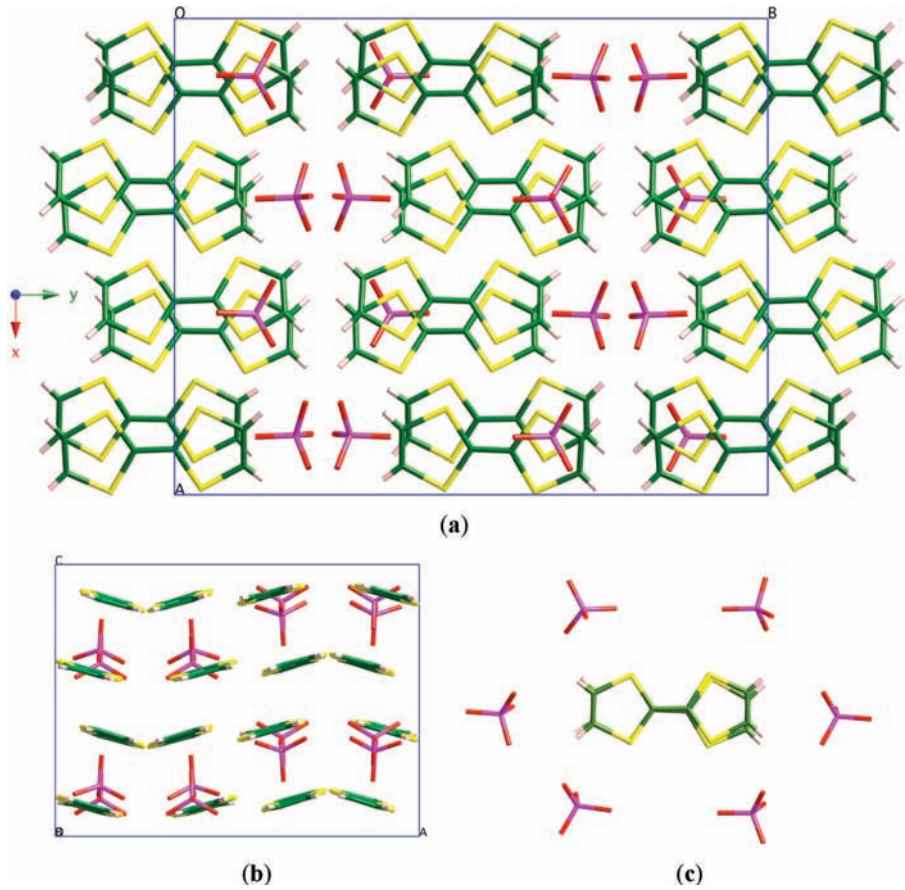

Figure 5. Views of the $[TTF]_2(ClO_4)_2$ (refs 11 and 12; S is yellow, C is green, Cl is magenta, H is white, and O is red) structure along the *c* and *b* axes (a and b), respectively. Also depicted is the view along the *c* axis of the six first-nearest neighbors of ClO_4^- anions that surround each $[TTF]_2^{2+}$ dimer, placed in the equatorial plane of each dimer (c).

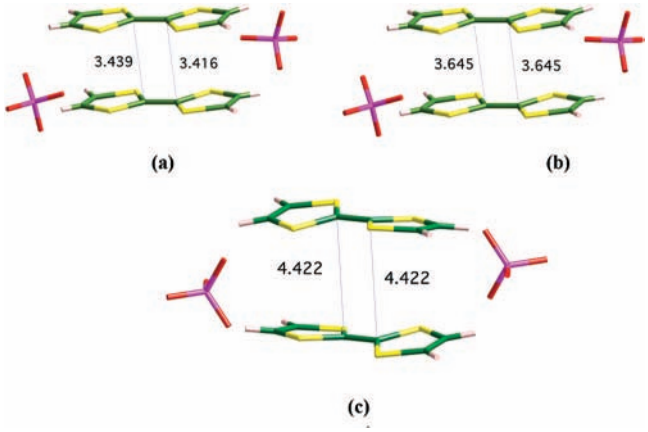

Figure 6. Geometry of the $[TTF]_2(ClO_4)_2$ (S is yellow, C is green, Cl is magenta, H is white, and O is red) and aggregate used to study the properties of $[TTF]_2^{2+}$ dimers: (a) crystal geometry, (b) optimum RB3LYP/6-31+G(d) geometry, and (c) optimum UB3LYP/6-31+G(d) geometry.

an indication of the validity of the use of $[TTF]_2(ClO_4)_2$ aggregates to study crystal properties. A RB3LYP vibrational analysis confirmed the minimum energy nature of the RB3LYP-level optimized geometry (all frequencies are positive, the smallest one being 23.3 cm^{-1}). When the $[TTF]_2(ClO_4)_2$ geometry optimization is done at the UB3LYP/6-31+G(d) level, Figure 6c, the shortest C···C distance is ~4.5 Å, too far away to allow the overlap of the SOMO orbitals of the two radical cations. Note that the optimum UB3LYP geometry is more stable than the optimum RB3LYP geometry, and the RB3LYP optimum geometry converts spontaneously into the UB3LYP minimum when the double occupancy restriction imposed in RB3LYP-level calculations is relaxed. Therefore, the B3LYP functional fails to reproduce the observed diamagnetic ground state for $[TTF]_2(ClO_4)_2$.[20,21,48]

The electronic properties of the $[TTF]_2(ClO_4)_2$ aggregates were also analyzed at its crystal (Figure 7) and optimum RB3LYP geometries (Supporting Information Figure S1). The analysis at the optimum UB3LYP geometry was not performed because at such separation the $[TTF]^+$ radicals do not overlap their SOMO and behave as isolated fragments. Despite the long interfragment C···C distance (≈3.5 Å) found in the crystal and RB3LYP geometries, and despite the repulsive character of the $[TTF]^{\bullet+}$···$[TTF]^{\bullet+}$ interaction, the highest occupied molecular orbital (HOMO) and lowest unoccupied molecular orbital (LUMO) orbitals of the aggregate originate from the bonding and antibonding combinations of the two $[TTF]^{\bullet+}$ SOMO orbitals. The HOMO → LUMO transition is the lowest energy absorption in the UV−vis spectra and it occurs at 11 050 cm^{-1} (905 nm) in B3LYP calculations.[49] The dimer $S_0 \rightarrow S_1$ absorption is reported to be at 13 950 cm^{-1} (717 nm)[19] and should be associated to the 12 000 and/or 15 000 cm^{-1} bands reported by polarized absorption in $[TTF]_2(ClO_4)_2$ [21] crystals. This assignment is consistent with that reported for other 1:1 and more complex mixed-valence salts,[19] where absorptions at 12 100 (826 nm) to 13 950 (717 nm) cm^{-1}, depending on the direction of the polarized radiation, are observed. This is the behavior expected if an interfragment C−C bond would exist between the two fragments. Thus, due to the cation$^+$···anion$^-$ interactions, the two $[TTF]^{\bullet+}$ cation radicals are at a distance

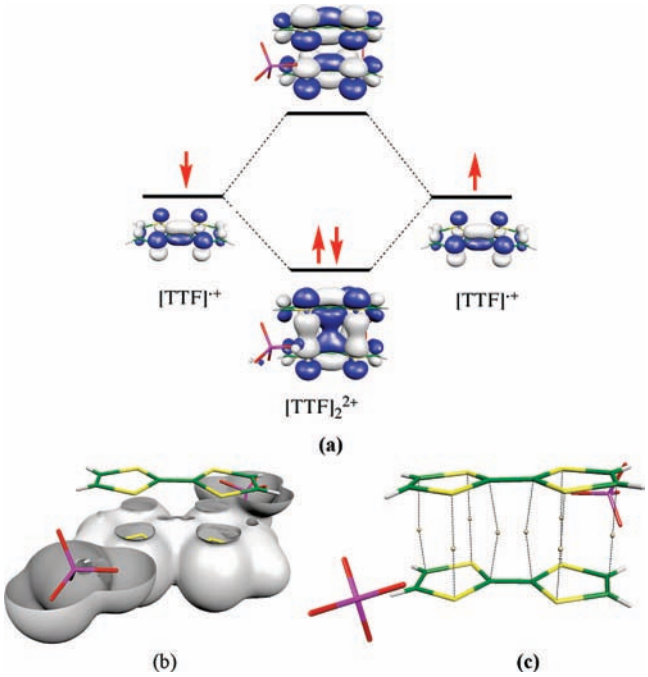

Figure 7. (a) MO diagram of the $[TTF]_2(ClO_4)_2$ aggregate (S is yellow, C is green, Cl is magenta, H is white, and O is red) at the crystal geometry, showing how the interaction of the two SOMO orbitals of the $[TTF]^{\bullet+}$ cation radicals generate the HOMO and LUMO of the aggregate; (b) isosurface of 0.05 au of electron density for the aggregate, showing the presence of funnels between the two cations, where the bond critical points are located; (c) position of the eight (four S···S and four C···C) intermolecular bond critical points in the aggregate (white).

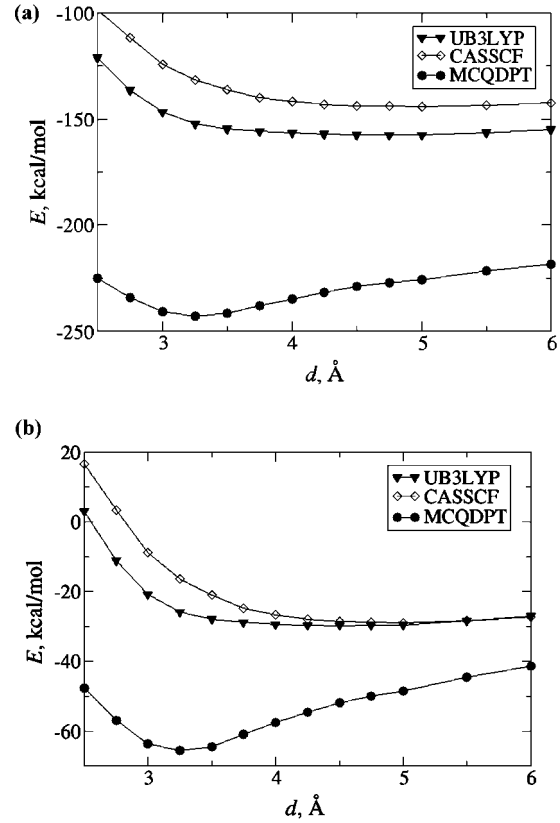

Figure 8. (a) Interaction energy curve, E, as a function of intradimer separation (d) for the dissociation computed at the UB3LYP, CASSCF(2,2), and MCQDPT/CASSCF(2,2) levels for the dissociation of a $[TTF]_2(ClO_4)_2$ aggregate in its singlet ground state into four fragments; (b) interaction energy curves, computed for the same aggregate and using the same methods, for the dissociation of the singlet state of the aggregate into two $[TTF]^{\bullet+}$ and two ClO_4^- ions in their optimum geometries.

where their SOMO orbitals overlap, and a long, multicenter bond between these two cation radicals forms.

An atoms-in-molecules (AIM) analysis[50] of the RB3LYP wave function was done as a tool to provide additional information with respect to the nature of the long intradimer $[TTF]_2^{2+}$ that arises from the overlap of the two $[TTF]^{\bullet+}$ SOMOs (stabilized by the electrostatic cation···anion interactions and helped by the dispersion component). From the location of the (3,−1) bond critical points that connects atoms within the $[TTF]_2^{2+}$ dimer, the $[TTF]^{\bullet+}\cdots[TTF]^{\bullet+}$ long bond involves two electrons and eight overlaps, or eight bonding components (Figure 7c and Supporting Information Figure S1). Four of these eight bonding components are C−C and four are S−S. These C−C components connect the central carbons and one of the five-membered rings carbon in each ring. The four S−S components involve the two sulfur atoms in each ring. At the optimum B3LYP/6-31+G(d) geometry, the electron density at the four C−C bond critical points and at the two critical points that connect the central C atoms is 4.5×10^{-3} atomic units (au) and 3.5×10^{-3} au in the five-membered ring carbons. Two of the S−S bond critical points (those involving the S atoms closest to the ClO_4^- anions) have an electron density of 11.2×10^{-3} au, while the other two have a density of 6.2×10^{-3} au. These values are close to those obtained in other long bonds.[1,10,11] The Laplacian for these eight bond critical points is negative. In addition to these intermolecular bond critical points, each perchlorate has one (3,−1) bond critical point with the S atom of each $[TTF]^{\bullet+}$ moiety, which is a manifestation of the ionic bond associated to the $[TTF]^{\bullet+}\cdots ClO_4^-$ interaction (this can be shown by looking at the density and positive Laplacian at the critical point in these ionic bonds).

Note that this AIM analysis is only indicative of the complex structure of the long bond between the $[TTF]^{\bullet+}$ species that compose the $[TTF]_2^{2+}$ dimers. This AIM analysis was done on the $[TTF]_2(ClO_4)_2$ aggregate to understand the nature of these bonds. In the $[TTF]_2(ClO_4)_2$ crystal each $[TTF]_2^{2+}$ is surrounded by six first-nearest neighbor perchlorate anions, not the two present in the $[TTF]_2(ClO_4)_2$ aggregate used as the charge-neutral model for the computational study. The four additional perchlorate anions in the unit cell lead to the further disappearance of the two C−C bond critical points associated to the external five-membered rings (due to the distortion induced in the wave function by the new $cation^+\cdots ClO_4^-$ ionic bonds similar to what is computed for the two perchlorates used in the computational model).

In order to check the quality of the previous B3LYP results for the $[TTF]_2(ClO_4)_2$ aggregate, computations were also done at the MCQDPT/CASSCF(2,2) level, which also uses the 6-31+G(d) basis set. Here the interaction energy curve for the dissociation of the aggregate into its four fragments was computed for the singlet ground state as a function of the shortest interfragment C···C distance (Figure 8a). At each point the geometry was first optimized at the UB3LYP/6-31+G(d) level, and the interaction energy was computed as the difference between the aggregate energy at the point and the energy of the fragments at a distance of 200 Å from the center of mass (each fragment at its optimum isolated geometry). The CASSCF(2,2) curve is nearly parallel to the UB3LYP curve and is ∼25 kcal/mol less stable, Figure 8a. The minimum of the curve occurs at a C···C distance of ∼4.5 Å; however, the MCQDPT/CASSCF(2,2) curve has a more stable minimum at 3.24 Å. An

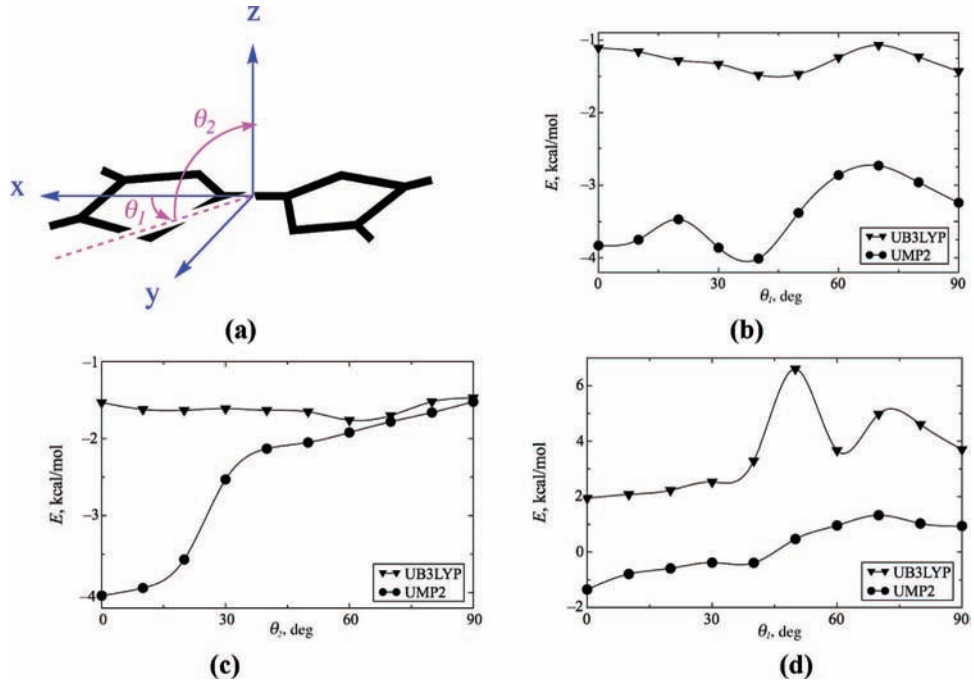

Figure 9. (a) Relative orientations of the $[TTF]^{\bullet+}$ and CH_2Cl_2 molecules, (b) interaction energy computed for the scan along the $x-y$ plane in the C−Cl···$[TTF]^{\bullet+}$ orientation, (c) interaction energy computed in the C−Cl···$[TTF]^{\bullet+}$ orientation for the scan along the $y-z$ plane when $\theta_1 = 40°$, and (d) interaction energy computed for the scan along the $x-y$ plane in the C−H···$[TTF]^{\bullet+}$ orientation.

analysis of the occupation of the CASSCF(2,2) wave function indicates that the HOMO and LUMO orbitals (that build the CAS space) have an occupation of 1.69 and 0.31 electrons, respectively (the shape of the CASSCF(2,2) active orbitals is plotted in Supporting Information Figure S2). Therefore, the MCQDPT/CASSCF(2,2) calculated singlet ground state is mostly closed-shell, with a non-negligible open-shell contribution. The MCQDPT/CASSCF(2,2)-computed first excited state (S_1) is mostly dominated by the open-shell singlet, in accord with the qualitative assignment of the observed electron absorption spectrum[19] based on the aforementioned qualitative MO diagram (Figure 7a).

The interaction energy curve for the dissociation of the $[TTF]_2(ClO_4)_2$ aggregate into two $[TTF]^{\bullet+}$ and two ClO_4^- ions was also recomputed at the MCQDPT/CASSCF(2,2) level for the singlet state (Figure 8b). At each point the geometry was first optimized at the UB3LYP/6-31+G(d) level, and the interaction energy was computed as the difference between the aggregate energy at the point and the energy of two $[TTF]^{\bullet+}$ and two ClO_4^- ions at a distance of 200 Å from the center of mass (each moiety at its optimum isolated geometry). As in Figure 8a, the MCQDPT/CASSCF(2,2) calculations predict a singlet ground state for the $[TTF]_2(ClO_4)_2$ aggregate, which is more stable than that found by the B3LYP or CASSCF(2,2) methods. This indicates that the correlation energy significantly contributes to the stability of these aggregates. In other words, the long bonds found between the $[TTF]_2^{2+}$ dimers in these aggregates are mostly electrostatic but with a relevant correlation contribution.

3. Nature of the [TTF]···$[TTF]^{\bullet+}$ Interactions in Solution. The existence of $[TTF]_2^{2+}$ dimers in solution (acetonitrile, methanol, ethanol, acetone, DMF, THF, dichloromethane) is well established.[34−36] However, the small enthalpy of formation of these dimers in solution (−3.8 to −9.1 kcal/mol; −3.8 kcal/mol in dichloromethane[36]) indicates that it cannot be associated to $[TTF]_2^{2+}(anion^-)_2$ aggregates, whose stability would be much larger and also solvent-independent. Besides, the presence of dimers in solution has been detected at millimolar concentrations, and in low concentration solutions, the anions and anions are solvent-separated and are too distant to form $[TTF]_2^{2+}(anion)_2$ aggregates. Therefore, a stabilizing interaction that compensates the $[TTF]^{\bullet+}$···$[TTF]^{\bullet+}$ repulsion and allows the formation of $[TTF]_2^{2+}$ dimers needs to be identified. The most likely option is formation of $[TTF]_2^{2+}(solvent)_n$ solvates. Therefore, solvates of $[TTF]_2^{2+}(solvent)_n$ composition, as already reported for $[TCNE]_2^{2-}(solvent)_n$,[51] among other aggregates, should form in solution.[52] The stability of these aggregates comes from the $[TTF]^{\bullet+}$···solvent interactions, which should exceed the $[TTF]^{\bullet+}$···$[TTF]^{\bullet+}$ repulsion, thus stabilizing the formation of $[TTF]_2^{2-}$ dimers in solution. The validity of this approach for $[TTF]_2^{2+}(CH_2Cl_2)_n$ aggregates, experimentally the weakest of all reported $[TTF]_2^{2-}$ dimers in solution, is described below.[36]

The first step in this study was the evaluation of the strength and directionality of the $[TTF]^{\bullet+}$···CH_2Cl_2 interaction; hence, the interaction energy of a $[TTF]^{\bullet+}$···CH_2Cl_2 complex was computed at the UB3LYP/6-31+G(d) and UMP2/6-31+G(d) levels. Two orientations were employed to explore the whole range of interaction energies (Figure 9a): the $x-y$ in-plane and $y-z$ out-of-plane orientations. Along each of these directions, two possible orientations of the CH_2Cl_2 were explored: one where one C−Cl bond of CH_2Cl_2 was forced to point toward the center of mass of $[TTF]^{\bullet+}$ (Figure 9, parts b and c), and one where one C−H bond points toward the center of mass of $[TTF]^{\bullet+}$ (Figure 9d). As the $x-y$ orientation indicates that the interaction is either energetically weakly attractive or repulsive, no attempt was made to compute the $y-z$ scan for this orientation. The C−Cl···$[TTF]^{\bullet+}$ orientation was found to be more stable in the $y-z$ scan. Therefore, the $y-z$ scan was not computed for the C−H···$[TTF]^{\bullet+}$ orientation.

The analysis of Figure 9, parts b and c, shows the presence of three local minima with energies in the 3−4 kcal/mol range at the UMP2 level, and in the 1−2 kcal/mol range at the B3LYP level, reflecting the importance of correlation in the

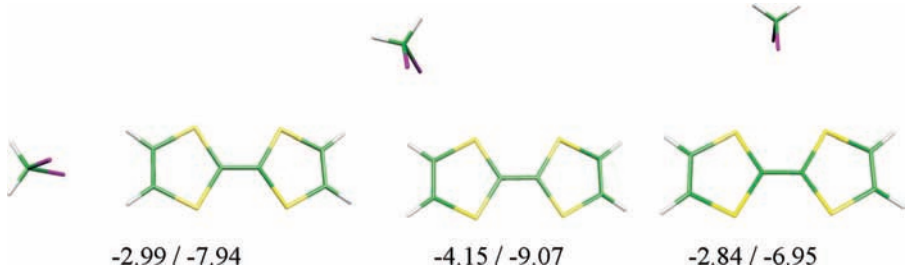

Figure 10. Different minimum energy conformations located in the potential energy surface of the $[TTF]^{\bullet+}\cdots CH_2Cl_2$ complex (S is yellow, C is green, Cl is magenta, and H is white). The numbers below each optimum structure are the B3LYP and UMP2 interaction energies computed using the 6-31+G(d) basis set.

$[TTF]^{\bullet+}\cdots CH_2Cl_2$ interaction. On the basis of these three local minima, the geometry was optimized, Figure 10. The most stable of these structures gives a best estimate of the $[TTF]^{\bullet+}\cdots CH_2Cl_2$ interaction energy of −4.5 kcal/mol per C−Cl···$[TTF]^{\bullet+}$ interaction (Figure 10, middle). As each CH_2Cl_2 molecule can make two C−Cl···$[TTF]^{\bullet+}$ interactions, four solvent molecules (−36 kcal/mol) are needed to overcome the $[TTF]^{\bullet+}\cdots[TTF]^{\bullet+}$ repulsion (∼27.5 kcal/mol). Starting from various initial structures designed to maximize the simultaneous interactions per solvent molecule per two $[TTF]^{\bullet+}$ cations, the most stable structure of the $[TTF]_2^{2+}(CH_2Cl_2)_4$ aggregate was located via a RB3LYP/6-31+G(d) geometry optimization, Figure 11. This has the shortest intradimer C···C distance of 3.59 Å, in accord with that obtained using the same method for the $[TTF]_2^{2+}(ClO_4^-)_2$ aggregates. This minimum has $\sim D_{2h}$ symmetry, which was not imposed in the optimization. The HOMO and LUMO orbitals, which clearly resemble the electronic structure of the $[TTF]_2^{2+}$ dimers in crystals, are shown in Figure 11. The B3LYP minimum is metastable by 28 kcal/mol against the dissociation into its six constituents fragments. However, the metastability is likely due to deficiencies of the B3LYP functional that are corrected when using methods capable of providing a more accurate description of the dispersion component of the interaction energy. This possibility was explored by computing the interaction energy curve (Figure 12a) for the dissociation into its four fragments at the MCQDPT/CASSCF(2,2) at various C···C separations between the central atoms of $[TTF]^{\bullet+}$. The (2,2) active space is constituted by the HOMO and LUMO that results from combining the $[TTF]^{\bullet+}$ SOMO orbitals. The geometry of each point of the curve was taken as the optimum UB3LYP/6-31+G(d) one, imposing that the D_{2h} symmetry is preserved during these optimizations. The UB3LYP and CASSCF(2,2) curves are also given for comparison. The MCQDPT/CASSCF(2,2) calculations predict a minimum at 3.25 Å, with an interaction energy of −18.4 kcal/mol. At the UB3LYP and CASSCF(2,2) levels no minima are observed, once again reflecting the importance of correlation in the description of these aggregates (at the RB3LYP level there is a metastable minimum, but at this geometry the UB3LYP wave function has lower energy, and thus the minimum disappears at the UB3LYP level).

The electronic structures of the B3LYP and MCQDPT/CASSCF(2,2) wave functions were also analyzed (Figure 11 and 13, respectively), and they are identical to that found before for $[TTF]_2(ClO_4)_2$ aggregates. The bonding and antibonding combinations of the SOMO of the $[TTF]^{\bullet+}$ fragments are the two CASSCF(2,2) active orbitals with occupations of 1.67 and 0.33 electrons, respectively. Thus, the MCQDPT/CASSCF(2,2) ground state is a closed-shell singlet (S_0) with a non-negligible contribution from the open-shell singlet, whereas the first excited state (S_1) is mostly dominated by the open-shell singlet. This is

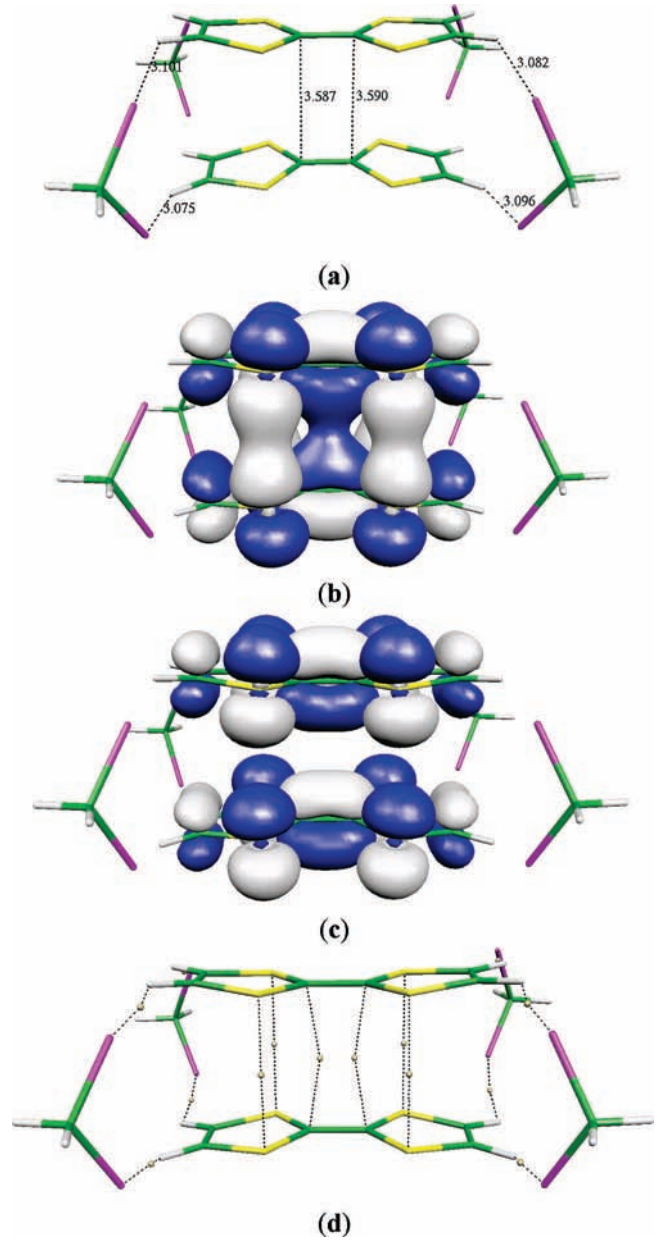

Figure 11. (a) Optimized RB3LYP/6-31+G(d) geometry of the $[TTF]_2^{2+}(CH_2Cl_2)_4$ aggregate (S is yellow, C is green, Cl is magenta, and H is white); (b) HOMO orbital of this aggregate at the RB3LYP/6-31+G(d) level; (c) LUMO orbital of this aggregate at the same level; (d) location of the six $[TTF]^{\bullet+}\cdots[TTF]^{\bullet+}$ and eight $[TTF]^{\bullet+}\cdots CH_2Cl_2$ bond critical points (white).

in accord with the qualitative assignment of the UV−vis spectrum based on the qualitative MO diagram (Figure 7a). Therefore, the electronic structure of the $[TTF]_2^{2+}$ dimers in

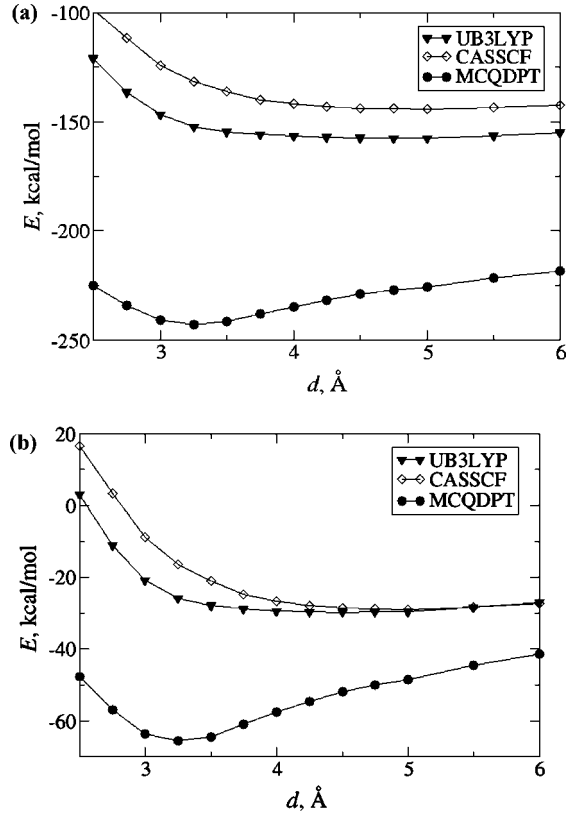

Figure 12. (a) Interaction energy curve, E, computed for the dissociation of the $[TTF]_2^{2+}(CH_2Cl_2)_4$ aggregate into its fragments using the UB3LYP, CASSCF(2,2), and MCQDPT2/CASSCF(2,2) methodologies, as a function of separation, d; (b) interaction energy curve computed for the dissociation of the $[TTF]_2^{2+}(CH_2Cl_2)_4$ aggregate into two $[TTF]^+(CH_2Cl_2)_2$ aggregates at their optimum B3LYP geometry using the UB3LYP, CASSCF(2,2), and MCQDPT/CASSCF(2,2) methodologies.

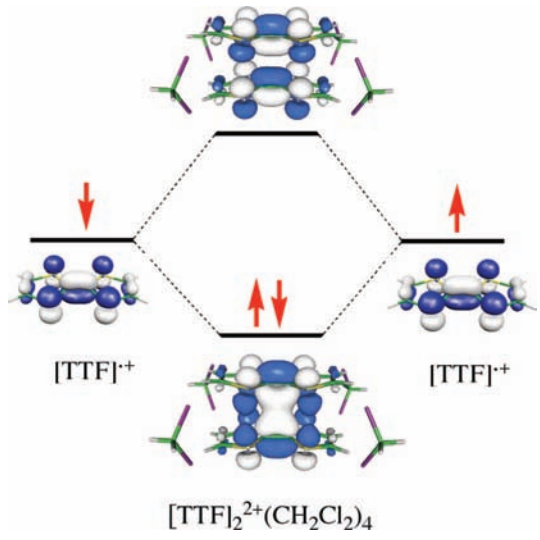

Figure 13. Electronic structure of the $[TTF]_2^{2+}(CH_2Cl_2)_4$ at the MCQDPT/CASSCF(2,2) wave function computed at its optimum geometry (see text) (S is yellow, C is green, Cl is magenta, and H is white).

solution is similar to that found in crystals and explains why the two UV−vis spectra are so similar.

An AIM analysis[50] on the RB3LYP and CASSCF(2,2) wave functions provides insight into the structure of the long bond in $[TTF]_2^{2+}(CH_2Cl_2)_4$ aggregates. There are six

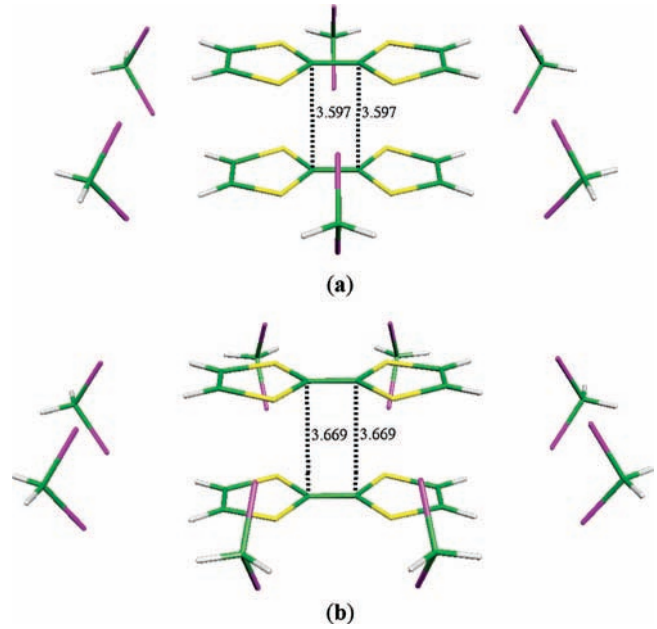

Figure 14. Optimized RB3LYP/6-31+G(d) geometry of the $[TTF]_2^{2+}(CH_2Cl_2)_6$ (a) and $[TTF]_2^{2+}(CH_2Cl_2)_8$ (b) aggregates (S is yellow, C is green, Cl is magenta, O is red, and H is white).

$[TTF]^{\bullet+}\cdots[TTF]^{\bullet+}$ bond critical points, two connecting C−C components and four connecting S−S components, Figure 11d.

Although at the MCQDPT/CASSCF(2,2) level the $[TTF]_2^{2+}(CH_2Cl_2)_4$ aggregate is stable against the dissociation into its six constituent fragments, Figure 12b, it is not stable against its dissociation into two $[TTF]^{\bullet+}(CH_2Cl_2)_2$ aggregates by 3.8 kcal/mol. Stability, however, is achieved by increasing the number of solvent molecules in the $[TTF]_2^{2+}(CH_2Cl_2)_n$ aggregate. Therefore, the stability of $[TTF]_2^{2+}(CH_2Cl_2)_6$ against both types of dissociation was explored. This aggregate was obtained by adding two CH_2Cl_2 molecules in the center of the cluster, Figure 14a. The geometry of this $[TTF]_2^{2+}(CH_2Cl_2)_6$ aggregate was optimized at the RB3LYP level by imposing a D_{2h} symmetry for the aggregate. A minimum was found (Figure 14a) where the shortest C···C distance is 3.60 Å. The MCQDPT/CASSCF(2,2) interaction energy at the $[TTF]_2^{2+}(CH_2Cl_2)_6$ optimum geometry was now computed, and again the active space is formed by the bonding and antibonding combinations of the $[TTF]^{\bullet+}$ SOMO orbitals. At the B3LYP level the $[TTF]_2^{2+}(CH_2Cl_2)_6$ aggregate is unstable against dissociation into eight fragments by 21.4 kcal/mol (22.1 kcal/mol was computed for an optimized $[TTF]_2^{2+}(CH_2Cl_2)_8$ aggregate, Figure 14b). However, the MCQDPT/CASSCF(2,2) interaction energy for the dissociation of $[TTF]_2^{2+}(CH_2Cl_2)_6$ into two $[TTF]^{\bullet+}{}_2(CH_2Cl_2)_3$ aggregates is −28.9 kcal/mol (the UB3LYP value is −8.5 kcal/mol). The last two values are indicative of a trend for $[TTF]^{\bullet+}$ monomers to form solvated $[TTF]_2^{2+}$ dimers. Note that other forms of dissociation of the solvated dimers are possible but are not expected to alter the main qualitative trend. Consequently, six is the minimum number of CH_2Cl_2 molecules that makes $[TTF]_2^{2+}$ stable in solution against fragmentation. In solution, the $[TTF]_2^{2+}$ dimers will be solvated by all molecules that form its first solvation shell (those solvent molecules directly attached to the solvate). The number of such solvent molecules has not been evaluated but is likely going to be eight or more that can be attached directly to the $[TTF]_2^{2+}$ dimer.

Conclusion

The existence of $[TTF]_2^{2+}$ dimers in crystals and in solution originates from $[TTF]^{\bullet+}\cdots$anion$^-$ or $[TTF]^{\bullet+}\cdots$solvent electrostatic interactions, whose sum the $[TTF]^{\bullet+}\cdots[TTF]^{\bullet+}$ repulsions for $[TTF]_2^{2+}(CH_2Cl_2)_4$ aggregates exceeds in solution, or the sum of the $[TTF]^{\bullet+}\cdots[TTF]^{\bullet+}$ and anion$^-\cdots$anion$^-$ repulsions, in $[TTF]_2(ClO_4)_2$ crystals. As shown by the results of the MCQDPT/CASSCF(2,2) calculations, the electronic ground state of the $[TTF]_2^{2+}$ dimers in these clusters is a closed-shell single state, with non-negligible contribution of the open-shell singlet. This ground state is not well reproduced in B3LYP or CASSCF(2,2) calculations, which predict an open-shell singlet ground state.

Acknowledgment. We thank Christopher Kareis and William W. Shum for sample preparation and magnetic studies. I.G.-Y. and J.J.N. were supported by the Spanish Science and Education Ministry (BQU2002-04587-C02-02, UNBA05-33-001, and Ph.D. Grant to I.G.-Y.) and the CIRIT (2001SGR-0044 and 2005-PEIR-0051/69). Computer time was also provided by CESCA and BSC. J.S.M. was supported in part by the U.S. NSF (Grant No. 0553573) and the DOE (Grant No. DE FG 03-93ER45504).

Supporting Information Available: MO diagram of the $[TTF]_2(ClO_4)_2$ aggregate, electron density and position of the eight intradimer intermolecular bond critical points in this aggregate, shape of the CASSCF(2,2) active orbitals, and full list of authors for ref 41. This material is available free of charge via the Internet at http://pubs.acs.org.

References and Notes

(1) Novoa, J. J.; Lafuente, P.; Del Sesto, R. E.; Miller, J. S. *Angew. Chem., Int. Ed.* **2001**, *40*, 2540.
(2) Del Sesto, R. E.; Miller, J. S.; Lafuente, P.; Novoa, J. J. *Chem. Eur. J.* **2002**, *8*, 4894.
(3) Novoa, J. J.; Lafuente, P.; Del Sesto, R. E.; Miller, J. S. *CrystEngComm* **2002**, *4*, 373.
(4) Lu, J.-M.; Rosokha, S. V.; Kochi, J. K. *J. Am. Chem. Soc.* **2003**, *125*, 12161.
(5) Jakowski, J.; Simons, J. *J. Am. Chem. Soc.* **2003**, *125*, 16089.
(6) Jung, Y.; Head-Gordon, M. *Phys. Chem. Chem. Phys.* **2004**, *6*, 2008.
(7) Miller, J. S.; Novoa, J. J. *Acc. Chem. Res.* **2007**, *40*, 189.
(8) Bagnato, J. D.; Shum, W. W.; Strohmeier, M.; Grant, D. M.; Arif, A. M.; Miller, J. S. *Angew. Chem., Int. Ed.* **2006**, *45*, 5326.
(9) Goto, G.; Kubo, T.; Yamamoto, K.; Nakazawa, S. K.; Sato, K.; Shiomi, D.; Takui, T.; Kubota, M.; Kobayshai, Y.; Yakusi, K.; Ouyang, J. A. *J. Am. Chem. Soc.* **1999**, *121*, 1619.
(10) Garcia-Yoldi, I.; Miller, J. S.; Novoa, J. J. *J. Phys. Chem. A* **2007**, *111*, 8020.
(11) Garcia-Yoldi, I.; Mota, F.; Novoa, J. J. *J. Comput. Chem.* **2007**, *28*, 326.
(12) Garcia-Yoldi, I.; Miller, J. S.; Novoa, J. J. *Phys. Chem. Chem. Phys.* **2008**, *10*, 4106.
(13) Reis, A. H., Jr.; Gebert, E.; Miller, J. S. *Inorg. Chem.* **1981**, *20*, 313.
(14) Goldberg, S. Z.; Spivack, B.; Stanley, G.; Eisenberg, R.; Braitsch, D. M.; Miller, J. S.; Abkowitz, M. *J. Am. Chem. Soc.* **1977**, *99*, 110.
(15) Grossel, M. C.; Evans, F. A.; Hriljac, J. A.; Prout, K.; Weston, S. C. *J. Chem. Soc., Chem. Commun.* **1990**, 1494.
(16) Axcondo, M. T.; Ballester, L.; Golhen, S.; Gutierrez, A.; Ouahab, L.; Yartsev, S.; Delhaes, P. *J. Mater. Chem.* **1999**, *9*, 1237.
(17) Hynes, R. C.; Morton, J. R.; Preston, K. F.; Williams, A. J.; Evans, F.; Grossel, M. C. L.; Sutcliffe, H.; Weston, S. C. *J. Chem. Soc., Faraday Trans.* **1991**, *87*, 2229.
(18) Miller, J. S.; Zhang, J. H.; Reiff, W. M.; Preston, L. D.; Reis, A. H., Jr.; Gerbert, E.; Extine, M.; Troup, J.; Ward, M. D *J. Phys. Chem.* **1987**, *91*, 4344.
(19) Torrance, J. B.; Scott, B. A.; Welber, B.; Kaufman, F. B.; Seiden, P. E. *Phys. Rev. B* **1979**, *19*, 730.
(20) Yakushi, K.; Nishimura, S.; Sugano, T.; Kuroda, H. *Acta Crystallogr., Sect. B* **1980**, *36*, 358.
(21) Sugano, T.; Kuroda, H.; Yakushi, K. *Bull. Chem. Soc. Jpn.* **1978**, *51*, 1041.
(22) Yamashita, A.; Akutsu, H.; Yamada, J.; Nakatsuji, S. *Polyhedron* **2005**, *24*, 2796.
(23) Matsubayashi, G.; Ueyama, K.; Tanaka, T. *J. Chem. Soc., Dalton Trans.* **1985**, 465.
(24) Furuta, K.; Akutsu, H.; Yamada, J.; Nakatsuji, S. *Synth. Met.* **2005**, *152*, 381.
(25) Morgado, J.; Santos, I. C.; Veiros, L. F.; Rodrigues, C.; Henriques, R. T.; Duarte, M. T.; Alcacer, L.; Almeida, M. *J. Mater. Chem.* **2001**, *11*, 2108.
(26) Libage, C.; Fourmigue, M.; Batail, P.; Canadell, E.; Coulon, C. *Bull. Soc. Chim. Fr.* **1993**, *130*, 761.
(27) Yamochi, H.; Konsha, A.; Saito, G.; Matsumoto, K.; Kusunoki, M.; Sakaguchi, K. *Mol. Cryst. Liq. Cryst. Sci. Technol., Sect. A* **2001**, *350*, 265.
(28) Akutsu, H.; Masaki, M.; Mori, K.; Yamada, J.; Nakatsuji, S. *Polyhedron* **2005**, *24*, 2126.
(29) Giffard, M.; Mabon, G.; Leclair, E.; Mercier, N.; Allain, M.; Gorgues, A.; Molinie, P.; Neilands, O.; Krief, P.; Khodorkowsky, V. *J. Am. Chem. Soc.* **2001**, *123*, 3852.
(30) Slougui, A.; Ouahab, L.; Perrin, C.; Grandjean, D.; Batail, P. *Acta Crystallogr., Sect. C* **1989**, *45*, 388.
(31) Teitelbaum, R. C.; Marks, T. J.; Johnson, C. K. *J. Am. Chem. Soc.* **1980**, *102*, 2986.
(32) Coronado, E.; Galan-Mascaros, J. R.; Gimenez-Sais, C.; Gomez-Garcia, C. J.; Ruiz-Perez, C.; Triki, S. *Adv. Mater.* **1996**, *8*, 737.
(33) Bondi, A. *J. Phys. Chem.* **1964**, *68*, 441.
(34) Benz, M. E.; Tabakovic, I.; Millar, L. L. *Chem. Mater.* **1994**, *6*, 351.
(35) Khodorkovsky, V.; Shapiro, L.; Krief, P.; Shames, A.; Mabon, G.; Gorgues, A.; Giffard, M. *Chem. Commun.* **2001**, 2736.
(36) Rosokha, S. V.; Kochi, J. K. *J. Am. Chem. Soc.* **2007**, *129*, 828.
(37) B3LYP is a density functional obtained by taking the three-parameter nonlocal exchange funcional of Becke and the nonlocal correlation functional of Lee−Yang−Parr: (a) Becke, A. D. *J. Chem. Phys.* **1993**, *98*, 5648. (b) Lee, C.; Yang, W.; Parr, R. G. *Phys. Rev. B* **1988**, *37*, 785.
(38) Nakano, H.; Nakayama, K.; Hirao, K.; Dupuis, M. *J. Chem. Phys.* **1997**, *106*, 4912.
(39) Roos, B. O.; Andersson, K.; Fulscher, M. K.; Malmqvist, P.-A.; Serrano-Andres, L.; Pierloot, K.; Merchan, M. *Adv. Chem. Phys.* **1996**, *93*, 219.
(40) A basis set built by adding diffuse functions to the 6-31G(d) basis set. The latter is described in: Ditchfield, R.; Hehre, W. J.; Pople, J. A. *J. Chem. Phys.* **1971**, *54*, 724.
(41) Frisch, M. J.; et al. Gaussian-03, revision-C.02; Gaussian, Inc.: Wallingford, CT, 2004.
(42) Schmidt, M. W.; Baldridge, K. K.; Boatz, J. A.; Elbert, S. T.; Gordon, M. S.; Jensen, J. H.; Koseki, S.; Matsunaga, N.; Nguyen, K. A.; Su, S. J.; Windus, T. L.; Dupuis, M.; Montgomery, J. A. *J. Comput. Chem.* **1993**, *14*, 1347.
(43) Boys, S. F.; Bernardi, F. *Mol. Phys.* **1970**, *19*, 553.
(44) The validity of the counterpoise method for correcting the BSSE was demonstrated analytically in ref 45 and numerically in ref 46.
(45) van Duijneveldt, F. B.; van Duijneveldt-van de Rijdt, J. G. C. M.; van Lenthe, J. H. *Chem. Rev.* **1994**, *94*, 1873.
(46) Novoa, J. J.; Planas, M.; Whangbo, M.-H. *Chem. Phys. Lett.* **1994**, *225*, 240.
(47) Allen, F. H. *Acta Crystallogr., Sect. B* **2002**, *58*, 380.
(48) $[TTF]_2[ClO_4]_2$ is diamagnetic below 400 K with no evidence of population of its triplet excited state.
(49) This is a qualitative estimate obtained by looking a the energy difference in the canonical orbitals. Although the LUMO energy is not a well-defined property in Hartree−Fock and DFT calculations, the values obtained when canonical orbitals are used provide physically meaningful estimates of energy HOMO−LUMO differences in many cases.
(50) Bader, R. F. *Atoms in Molecules: A Quantum Theory*; Clarendon Press: Oxford, New York, 1990.
(51) Garcia-Yoldi, I.; Miller, J. S.; Novoa, J. J. *J. Phys. Chem. A* **2007**, *111*, 8020.
(52) Carvajal, M. A.; García-Yoldi, I.; Novoa, J. J. *J. Mol. Struct. (THEOCHEM)* **2005**, *727*, 181.

JP807022H